RESEARCH ARTICLE

BRITISH ECOLOGICAL SOCIETY | Functional Ecology

Temperature constraints of terrestrial ecosystem respiration in global biomes

Zhenhai Liu[1,2,3] (ORCID) | Jiquan Chen[3] | Bin Chen[1] | Shaoqiang Wang[1,2,4,5]

[1]Key Laboratory of Ecosystem Network Observation and Modeling, Institute of Geographic Sciences and Natural Resources Research, Chinese Academy of Sciences, Beijing, China

[2]College of Resources and Environment, University of Chinese Academy of Sciences, Beijing, China

[3]Department of Geography, Environment, and Spatial Sciences, Michigan State University, East Lansing, Michigan, USA

[4]Hubei Key Laboratory of Regional Ecology and Environmental Change, School of Geography and Information Engineering, China University of Geosciences, Wuhan, China

[5]Technology Innovation Center for Intelligent Monitoring and Spatial Regulation of Land Carbon Sequestrations, Ministry of Natural Resources, Wuhan, China

Correspondence
Bin Chen
Email: chenbin@igsnrr.ac.cn

Abstract

1. Ecosystem respiration (Re) plays a critical role in the global carbon cycle, but is conventionally modelled with temperature response functions that do not adequately account for the limiting effects of high temperature on Re.

2. Using Re data from the FLUXNET2015 network, we compared the conventional exponential temperature response function with a unimodal function that incorporates these effects.

3. We found that the conventional function significantly underestimates the sensitivity of Re to temperature, potentially leading to overestimation of future carbon emissions. The activation energy (E_a) estimated by the unimodal function averaged 0.97 ± 0.44 eV, substantially higher than the 0.58 ± 0.27 eV calculated by the exponential function. The temperature threshold (T_{th}) for Re inhibition was identified at an average of 26.58°C across biomes. The largest Re increase occurs under SSP585, reaching 147.85% and 153.81% for the exponential and unimodal functions, respectively, by 2100 relative to Re simulated using the exponential function in 1990. As rising temperatures push ecosystems toward their thermal optimum, greater overestimation beyond the divergence threshold in SSP585 reduces the difference between the two functions compared to SSP245 and SSP370.

4. These findings emphasize an underestimated temperature dependence and inaccurate trends in ecosystem respiration, highlighting the necessity of integrating high-temperature inhibition effects into Re models to improve projections of carbon dynamics.

KEYWORDS
ecosystem respiration, high-temperature inhibition, temperature dependence, temperature response function, temperature threshold

1 | INTRODUCTION

Ecosystem respiration (Re) is a fundamental process in the global carbon cycle, involving the release of CO_2 from plants and soils back to the atmosphere (Atkin & Tjoelker, 2003; Maes et al., 2024). Re and ecosystem gross primary production (GPP) through photosynthesis jointly determine the carbon balance of terrestrial ecosystems, commonly referred to as net ecosystem production

(NEP) (Chen, 2021; Schimel et al., 2001). Recent studies have demonstrated that the release of CO_2 from terrestrial ecosystems has been increasing and is likely to continue to rise in the future (Duffy et al., 2021; Tang et al., 2022; Yu et al., 2022). Temperature is typically considered as the primary driver of Re and its changes over time (Davidson & Janssens, 2006; Niu et al., 2024; Tagesson et al., 2024), but mounting evidence shows that temperature has not been adequately formulated in Re models at local, biome, and global scales (Bond-Lamberty & Thomson, 2010; Chen et al., 2023; Zou et al., 2022). This limitation hinders our capability to estimate total carbon emissions as well as the carbon balances of terrestrial ecosystems under the changing climate, especially with the increasing frequency of extremely high temperatures (Bennett et al., 2023; Qu et al., 2024).

Conventional schools of thought on the temperature dependence of Re assume an exponential rise in Re with temperature, and that it will continue to increase in the foreseeable warmer future (Duffy et al., 2021; Nissan et al., 2023; Yu et al., 2022). However, metabolic rates for plant photosynthesis and respiration are known to increase with temperature, reaching a threshold (i.e. temperature constraint) after which these rates start to decline (Atkin et al., 2000; Kattge & Knorr, 2007; Lloyd & Taylor, 1994; Michaletz, 2018; O'Sullivan et al., 2017). For many terrestrial regions, ambient air temperatures during the warmest quarter are often thought to have surpassed the temperature threshold (T_{th}) for photosynthesis (~23 ± 6°C) (Bennett et al., 2021; Duffy et al., 2021; Huang et al., 2019). Similarly, respiration rates have been observed to decline sharply at high temperatures (Duffy et al., 2021; O'Sullivan et al., 2017; Robinson et al., 2017; von Buttlar et al., 2018; Zou et al., 2022), with laboratory experiments estimating the T_{th} for leaf and soil respiration to be around 50 and 70°C, respectively (Liang et al., 2018; Robinson et al., 2017). These laboratory-based T_{th} values, however, far exceed the T_{th} observed in the field (e.g. in-situ measured T_{th} for soil respiration is approximately 20°C at Canada forest sites; Khomik et al., 2009) and the projected temperature of any near-term warming scenario. The temperature inhibition of Re has also been widely reported in the literature (Chen et al., 2023; Niu et al., 2024; Ping et al., 2023). Were future carbon release predicted based on these laboratory-based temperature thresholds, with the expectation that Re will continue to increase within the projected temperature range, our current estimates would be significantly overstated under warmer scenarios.

The temperature dependence of Re, traditionally quantified using the exponential Boltzmann-Arrhenius (B-A) function, describes how Re rate varies with temperature in terrestrial and aquatic biomes (Lloyd & Taylor, 1994; Reichstein et al., 2005; Yvon-Durocher et al., 2012). When T_{th} is higher than the ambient temperature, the B-A function appears to be reliable (Figure 1a). However, this monotonic function describing the unimodal Re with temperature exceeding T_{th} is problematic (Figure 1b). Johnston et al. (2021) recognized the limits of traditional models in assessing temperature dependence and applied a segmented threshold model with Re data from the FLUXNET2015 database. They found a lowered temperature dependence of Re at higher temperatures, with a breakpoint at 15.1 ± 0.22°C. Based on the FLUXNET-CH_4 database, Li et al. (2023) also reported that the temperature dependence of Re was reduced with rising monthly mean temperature, reasoning that high summer temperatures inhibit Re. An increasing number of similar studies support the abovementioned findings in different biomes (Chen, 2021; Xu & Qi, 2001; Zou et al., 2022). The B-A function is widely used in popular ecosystem models (Todd-Brown et al., 2013) and as a standard flux partitioning procedure for the data process of FLUXNET, OzFlux, and other networks, potentially leading to biased estimates (Isaac et al., 2017; Lasslop et al., 2010; Pastorello et al., 2020). Without doubt, it is necessary to seek a new temperature response function to improve the temperature sensitivity of Re for terrestrial ecosystems worldwide.
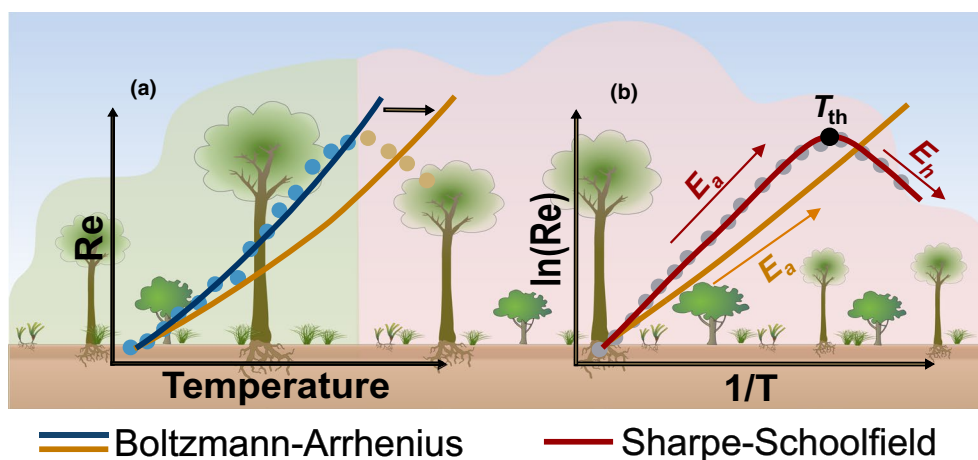

FIGURE 1 Changes in ecosystem respiration rate with temperature. (a) Re rate increases as an exponential function of temperature (blue points and line) until a temperature threshold is reached (brown points and line). (b) A monotonically increasing function that does not consider high-temperature inhibition would underestimate the activation energy, whereas the unimodal function (red points and line) provides realistic predictions. Re, ecosystem respiration; ln(Re), natural logarithm of Re; T_{th}, temperature threshold; 1/T, reciprocal of temperature; E_a, activation energy; E_h, deactivation energy.

Here, we reassessed the temperature response characteristics of Re by seeking answers to two fundamental questions: (i) What is the magnitude of underestimation using the actual temperature dependence of Re in exponential temperature response function across diverse biomes? (ii) How do unimodal temperature responses affect the projected trends for Re on a warming Earth? Firstly, we reevaluated the temperature dependence of Re in all Koppen-Geiger climatic biomes based on activation energy (E_a) through fitting a unimodal temperature response function (Sharpe-Schoolfield function, S-S) to the FLUXNET2015 Re data. This approach implicitly combines multiple rate-limiting processes, offering a comprehensive perspective on ecophysiology. We then underscored the limitations of the B-A function in estimating temperature response at extremely high temperatures based on eight sites with apparent heatwaves. Additionally, we analysed the contributions of other biophysical factors on model coefficients by biome. Finally, we examined the future trends of global land ecosystem respiration with projected temperatures at a global scale.

2 | MATERIALS AND METHODS

2.1 | Data sources

FLUXNET is a global network of eddy-covariance (EC) flux towers that record continuous exchanges of CO_2, water vapour, and energy between terrestrial ecosystems and the atmosphere (Baldocchi et al., 2001). FLUXNET2015 is the most updated dataset drawn from FLUXNET towers that provide daily mean air temperature and Re from 213 sites (Figure 2). These sites span a latitudinal range from 78.92°N to 37.43°S, encompassing polar to tropical rainforest biomes, with site air temperatures ranging from −52.88 to 46.26°C, based on FLUXNET2015 data.

The FLUXNET2015 sites were aggregated based on the Koeppen-Geiger climate classification (1986–2010) (Rubel et al., 2017). Biomes with fewer than five sites were merged into similar higher-level climatic zones. In the absence of such zones, we used the original classification. All sites were grouped into 12 biomes (Figure 2): A (tropical climates), BWh/BSh (arid and hot climates), BWk/BSk (arid and cold climates), Csa (temperate climates with dry and hot summer), Csb (temperate climates with dry and warm summer), Cfa (temperate climates without dry season and with hot summer), Cfb (temperate climates without dry season and with warm summer), Dw (cold climates with dry winter), Dfa (cold climates without dry season and with hot summer), Dfb (cold climates without dry season and with warm summer), Dfc (cold climates without dry season and with cold summer) and ET (polar climates). It is worth noting that most sites were in the mid-latitude biomes, with cold climate biomes having the highest number of sites (96 sites), and tropical climate biomes having the fewest (17 sites).

The FLUXNET2015 datasets were quality-controlled, filtered, gap-filled, and partitioned using consistent methods (Papale, 2020; Pastorello et al., 2020). To avoid self-correlation between GPP and Re caused by flux partitioning of eddy-covariance (EC) carbon fluxes (Vickers et al., 2009), we used Re and GPP data based on the daytime partition approach (Lasslop et al., 2010). This approach is based on a hyperbolic light response curve fit to daytime CO_2 flux, modified to account for the temperature sensitivity of respiration. In this study, we used non-gap-filled daily Re (RECO_DT_VUT_REF) and daily mean air temperature (TA_F) during the growing seasons for the temperature response of Re. Data were included only if quality control scores met thresholds of NEE_VUT_ReF_QC >0.8 and TA_F_QC >0.8. The growing season was defined as the periods when daily mean air temperature (T_a) exceeded 5°C for at least five consecutive days (Chen et al., 2023).
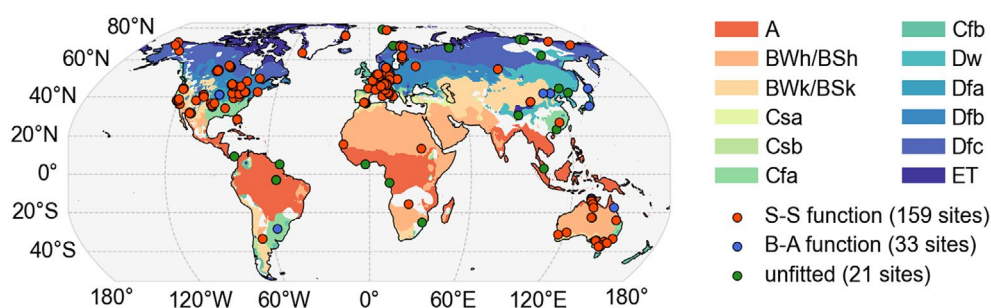

FIGURE 2 Distribution of FLUXNET2015 sites in Koppen-Geiger climate biomes (1986–2010) (Rubel et al., 2017). Among these sites, Re was better modelled with S-S function (red circles) at 159 sites and with the B-A function (blue circles) at 33 FLUXNET2015 sites. Re from 21 sites (green circles) did not show an apparent relationship with temperature. Biomes with fewer than five sites were merged into similar higher-level climatic zones. In the absence of higher-level climatic zones, we used the original classification. S-S function, Sharpe-Schoolfield function; B-A function, Boltzmann-Arrhenius function; A, tropical climates; BWh/BSh, arid and hot climates; BWk/BSk, arid and cold climates; Csa, temperate climates with dry and hot summer; Csb, temperate climates with dry and warm summer; Cfa, temperate climates without dry season and with hot summer; Cfb, temperate climates without dry season and with warm summer; Dw, cold climates with dry winter; Dfa, cold climates without dry season and with hot summer; Dfb, cold climates without dry season and with warm summer; Dfc, cold climates without dry season and with cold summer; ET, polar climates.

2.2 | Replication statement

Scale of inference	Scale at which the factor of interest is applied	Number of replicates at the appropriate scale
Biome	Biome	12 biomes
Site	Site	1 site per biome

2.3 | Temperature response function of Re

Two distinct temperature responses of Re were tested: B-A (Arrhenius, 1889) and S-S (Schoolfield et al., 1981) functions. The B-A function is expressed as

$$Re = Re_0 \cdot e^{-\frac{E_a}{kT}} \tag{1}$$

where Re (g C m^{-2}day^{-1}) is the daily ecosystem respiration, Re_0 (g C m^{-2}day^{-1}) is a normalization constant, E_a (eV) is the activation energy characterizing the temperature sensitivity of Re, k (8.617×10^{-5} eV K^{-1}) is the Boltzmann constant, and T (K) is the ambient temperature. The Boltzmann factor $e^{-E_a/kT}$ reflects the fraction of molecules that attain the E_a needed to react.

The S-S function assumes that reaction rates obey B-A kinetics at lower temperatures but are reduced by high-temperature inactivation. The S-S function is expressed as,

$$Re = Re_0 \cdot e^{-\frac{E_a}{kT}} \cdot \left[1 + \left(\frac{E_a}{E_h - E_a} \right) e^{-E_h \cdot \left(\frac{1}{kT_h} - \frac{1}{kT} \right)} \right]^{-1} \tag{2}$$

where E_h (eV) characterizes deactivation energy above the temperature T_h (K) at which the respiration is $1/2$ operational and $1/2$ dormant (Schoolfield et al., 1981). The T_{th} was defined as the temperature at the apex of the S-S unimodal curve.

The S-S function is a framework rooted in the principles of thermodynamics, which provides a mechanistic basis to simulate the temperature dependence of rates across scales from individual enzyme kinetics to organismal and ecosystem metabolism (Chen, 2021; Michaletz, 2018). The B-A function is a special case of the S-S function where the high-temperature inactivation term is one and the temperature-rate relationship is exponential without a maximum (Figure 1b; Schoolfield et al., 1981). The S-S function is applicable across a range of processes and levels of biological organization, and it has been widely applied to capture the temperature dependence of organismal growth (Adair et al., 1989; Gibert & De Jong, 2001; Padfield et al., 2020), plant photosynthesis (Michaletz, 2018; Stinziano et al., 2018), respiration (Padfield et al., 2016) and evolutionary patterns (Schaum et al., 2017).

Following Niu et al. (2012) and Chen et al. (2023), we grouped the daily mean air temperature and corresponding carbon fluxes (Re and GPP) into 1°C temperature bins for each site. The average value within each temperature bin was used to construct the $[Re - T_a]$ or $[GPP - T_a]$

response curves, emphasizing the variation of carbon fluxes with temperature. Fitting was performed using Levenberg–Marquardt nonlinear regression with Gaussian random starting values, followed by evaluation using the Akaike Information Criterion (AICc) (Akaike, 1998) from 20 fits for each curve. Model fitting was conducted in the statistic software R version 4.3.2 (R Core Team, 2023), utilizing a modified version of the code provided by Michaletz (2018). The starting value of parameters, E_a, and $\ln(Re_0)$, were estimated based on the data before T_{th}, which is estimated first and is the temperature when the carbon flux value reaching the maximum. E_a estimated using the linear regression between log (Re) and 1/kT. $\ln(Re_0)$ is the log transformed maximum Re. The starting value of T_h was set as the starting value of T_{th}. The starting value of E_h was set as the four times of starting value of E_a. These initial estimates were used to generate randomized starting values for each model parameter in each fitting iteration, using Gaussian distributions centered on the initial estimates. Each fit is based on the Levenberg–Marquardt nonlinear regression with a parameter search space described in Table S1.

2.4 | Inhibition of high temperature

Following the approach of Xu et al. (2020), who investigated the importance of high temperature at FLUXNET2015 sites (i.e. heatwave events), we selected eight sites based on similar criteria: (1) each site had over 7 years of meteorological measurements, (2) each site experienced at least three heatwave events in summer, (3) the selected sites represented a variety of ecosystem and plant functional types, (4) no irrigation was conducted during the study period. 'Hot days' were defined as days when the daily maximum temperature (T_{max}) ranked within the top 10% of historic daily T_{max} values and exceeded the multi-year average T_{max} by 5°C throughout the summer (mid-growing season) at a site. A period of at least seven consecutive 'hot days' was considered a heatwave event. If a 'non-hot day' occurred within a period of eight or more consecutive 'hot days,' the period was also classified as a heatwave event. Each vegetation type was represented by one site for our study, totalling eight sites, to assess the fitness of B-A and S-S functions for Re during hot years. The temperature dependence of Re was fitted with both functions during heatwave years.

2.5 | Importance of forcing factors

The Random Forest (RF) model enables us to assess the importance of meteorological, soil, and vegetation factors in estimated E_a^{Re}, T_{th}^{Re} and ΔE_a^{Re} (Gregorutti et al., 2017). E_a^{Re} and T_{th}^{Re} are derived from sites modelled with the S-S function; ΔE_a^{Re} represents the variance between the estimated E_a^{Re} in S-S and B-A functions.

Micrometeorological factors used in this study include the annual maximum daily temperature (T_{max}, °C), mean annual temperature (MAT, °C), growing season temperature (GST, °C), growing season solar radiation (GSR, W m^{-2}), annual precipitation (AP,

mm), vapour pressure deficit (VPD, kPa), potential evapotranspiration (PET, mm) and soil moisture (SM, $m^3 m^{-3}$). PET was calculated through the Thornthwaite method based on temperature and day length recorded by the EC tower (Adams, 2017; Chen, 2021). SM at 5 cm depth was obtained from the observation data of each site if available, or retrieved from the ESA CCI Soil Moisture Dataset by longitude and latitude (https://www.esa-soilmoisture-cci.org/) when SM was not measured at the tower site. All potential forcing variables were calculated from the site-year data. We considered soil properties such as soil organic carbon (SOC, $g kg^{-1}$), soil bulk density (BD, $kg m^{-3}$), soil nitrogen content (N, $cg kg^{-1}$) and pH obtained from SoilGrids (Poggio et al., 2021), as well as biomass (BM, $Mg C ha^{-1}$) (Liu et al., 2015) to evaluate their potential influences on E_a and T_{th}.

2.6 | Modelling Re

We applied the B-A and S-S functions to each Koppen-Geiger climatic biome to simulate Re for both historical (1990–2014) and future (2015–2100) periods under four climate scenarios. To construct these functions and estimate T_{th}, we utilized growing season data from FLUXNET2015, which were binned and averaged for each biome to ensure parameterization. The simulations of global terrestrial Re were conducted with surface temperature data from four climate change scenarios in the NoreSM2-MM model of Coupled Model Intercomparison Project 6 (CMIP6) (https://pcmdi.llnl.gov/CMIP6/): SSP126, SSP245, SSP370 and SSP585. The NoreSM2-MM model (Seland et al., 2020) operates at a daily or three-hour time step with a resolution of 1.25°×0.9375°. It implements a temperature response function for photosynthesis similar to the S-S model, with the response level indicated by E_a and E_h (Kattge & Knorr, 2007). For the temperature response function of Re in the NoreSM2-MM model, the Arrhenius function was employed (Ali et al., 2016). Land surface temperature data from NoreSM2-MM were used to drive both the B-A and S-S functions, enabling biome-specific simulations of Re under varying climate conditions.

3 | RESULTS

3.1 | Global biome E_a and T_{th}

The S-S function appeared to be superior to the B-A function for modelling the temperature responses of Re at 159 sites in the 12 Koppen-Geiger climate biomes (Figure 2). However, the B-A function provided a better fit for 33 sites. Both functions failed to capture temperature responses at 21 sites, mostly located in the equatorial region and Northeast Asia.

Estimated E_a in the S-S function at the 159 sites was considerably higher than that of the B-A function by biome (Figure 3a), with an average E_a^{S-S} and E_a^{B-A} of 0.97±0.44 eV and 0.58±0.27 eV, respectively (Table 1). Most sites (78.62%) have a difference between E_a^{S-S} and E_a^{B-A} (ΔE_a) ≤0.60 eV (Figure S1a). The relative E_a values from the two
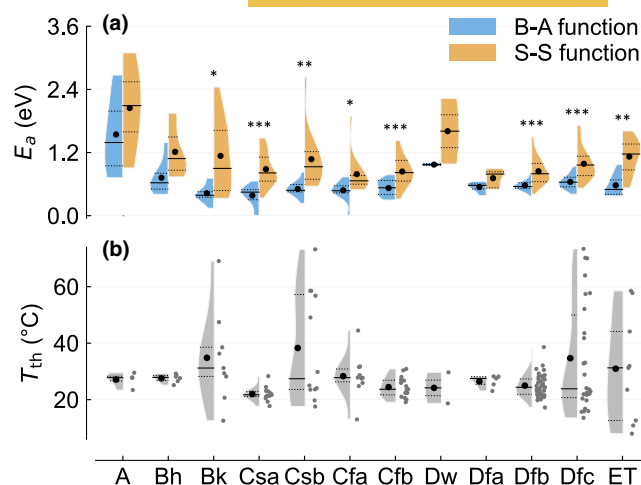

FIGURE 3 Violin plots of (a) activation energy and (b) temperature threshold by biome using B-A and S-S functions. Asterisks (*) indicate the significant difference between E_a^{B-A} and E_a^{S-S} (***$p<0.001$; **$p<0.01$; and *$p<0.05$). Bh and Bk represent BWh/BSh and BWk/BSk, respectively. See Figure 2 for biome names. Refer to Table 1 for the number of biome sites. S-S function, Sharpe-Schoolfield function; B-A function, Boltzmann-Arrhenius function; A, tropical climates; BWh/BSh, arid and hot climates; BWk/BSk, arid and cold climates; Csa, temperate climates with dry and hot summer; Csb, temperate climates with dry and warm summer; Cfa, temperate climates without dry season and with hot summer; Cfb, temperate climates without dry season and with warm summer; Dw, cold climates with dry winter; Dfa, cold climates without dry season and with hot summer; Dfb, cold climates without dry season and with warm summer; Dfc, cold climates without dry season and with cold summer; ET, polar climates; E_a, activation energy; T_{th}, temperature threshold.

functions among the biomes are nonetheless similar, with biomes in lower latitude regions having greater E_a than those in higher latitude areas (Figure S2a,b). Importantly, ΔE_a appears higher in mid-latitude biomes compared to high- and low-latitude biomes (Figure S2c).

The average T_{th} for Re across biomes ranges from 21.21 to 30.95°C in the S-S function, with a mean of 26.58°C (Figure 3b and Table 1). The T_{th} in 76.10% of the biomes falls between 15 and 35°C (Figure S3a), with 30.82% of sites showing a T_{th} that exceeds T_{max} (Figure S3b). Sites in low-latitude biomes exhibit a higher frequency of data exceeding the T_{th} (Figure S2e), but with T_{th} and T_{max} strongly and positively correlated ($r = 0.62$, $p < 0.001$) (Figure S3b). For sites where the B-A function fits better than the S-S function, there are fewer cases of temperature exceeding T_{th} (5.45% and 10.77% on average, respectively) (Table 1 and Table S2). It is worth noting that good performance of the B-A function indicates that ambient temperatures do not reach the T_{th} for the sites.

3.2 | Temperature inhibition of Re

The S-S function performed better than the B-A function at seven out of the eight sites that experienced heatwaves (Figure 4a–g), due to the presence of high-temperature inhibition of Re. The B-A

TABLE 1 Estimated model coefficients for sites with S-S function.

Biome	E_a^{B-A} (eV)	E_a^{S-S} (eV)	T_{th} (°C)	E_h^{S-S} (eV)	Post-threshold fraction (%)	AIC^{B-A}	AIC^{S-S}	n
A	1.54±0.87	2.05±0.92	27.12±2.62	11.00±7.64	31.47±6.05	−1.74±12.45	−22.31±18.28	4
BWh/BSh	0.72±0.34	1.21±0.50	27.57±1.50	5.19±3.37	32.92±14.03	8.60±19.32	−21.68±28.61	7
BWk/BSk	0.43±0.18	1.14±0.72	30.53±10.77	3.00±2.16	13.68±23.56	−24.80±32.50	−52.22±30.83	9
Csa	0.38±0.20	0.88±0.32	21.21±5.14	2.08±1.01	28.74±21.03	−8.39±29.18	−57.95±25.80	17
Csb	0.51±0.15	1.07±0.56	29.91±13.62	2.47±1.93	14.03±10.27	−25.64±24.50	−65.79±26.32	12
Cfa	0.48±0.19	0.79±0.39	28.32±7.72	2.83±2.34	16.72±19.05	−20.12±20.22	−57.44±27.41	11
Cfb	0.53±0.15	0.84±0.29	24.43±3.66	1.52±0.42	2.53±2.72	−39.88±29.68	−103.35±30.10	16
Dw	0.97±0.05	1.61±0.88	24.17±7.78	2.16±0.10	NA	−36.42±40.36	−51.16±21.02	2
Dfa	0.54±0.10	0.71±0.18	26.47±2.22	2.78±2.68	9.49±13.23	−34.71±22.45	−94.39±42.31	5
Dfb	0.57±0.11	0.84±0.25	26.33±7.30	1.86±1.00	4.04±5.96	−37.32±19.58	−90.35±33.82	41
Dfc	0.64±0.14	0.99±0.30	28.37±13.65	1.90±1.33	4.90±6.09	−32.26±19.37	−78.40±24.86	26
ET	0.58±0.21	1.12±0.35	30.95±17.42	3.12±3.94	6.79±10.33	−29.65±13.37	−74.55±21.25	9
All sites	0.58±0.27	0.97±0.44	26.58±9.33	2.51±2.55	10.77±15.45	−27.43±25.73	−73.96±35.22	159

Note: E_a^{B-A} and E_a^{S-S} represent estimated activation energy in the B-A and S-S functions, respectively. E_h^{S-S} indicates the deactivation energy in the S-S functions. Post-threshold fraction represents the percentage of data after the peak corresponding to the temperature threshold (T_{th}) in the S-S function. AIC^{B-A} and AIC^{S-S} represent the model accuracy for the B-A and S-S functions, respectively (AIC: Akaike information criterion). *n* represents the number of sites. See Figure 2 for biome names.
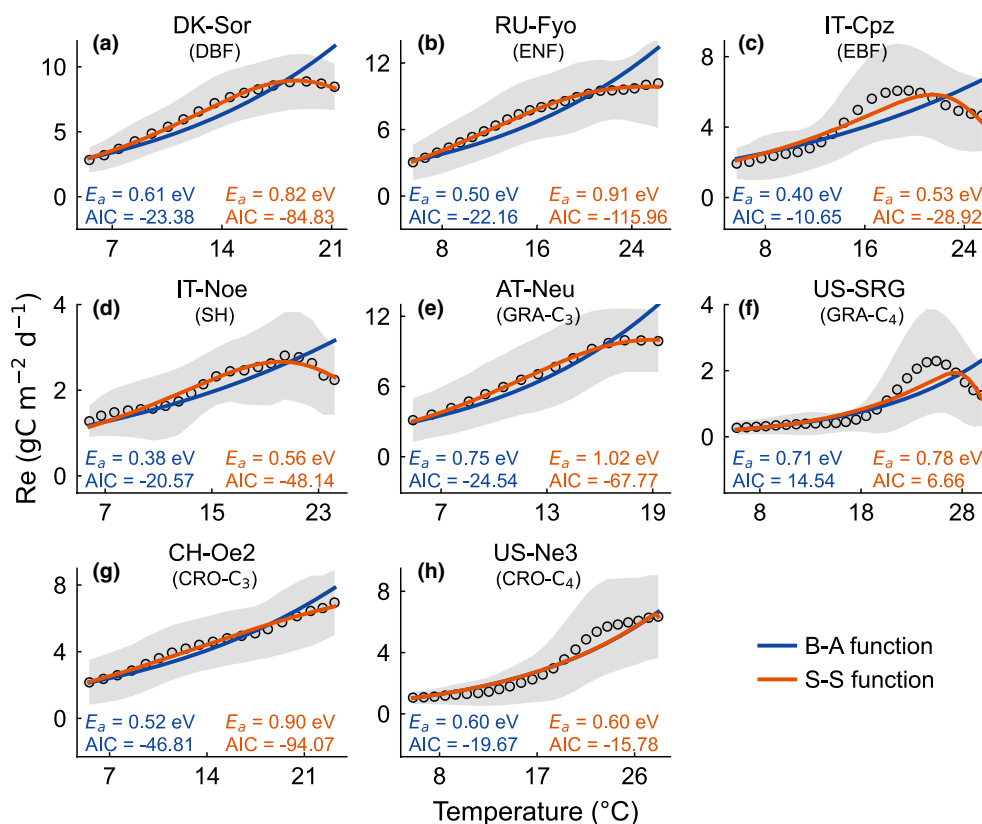

FIGURE 4 Thermal response curves of ecosystem respiration during heatwave years at eight selected sites: (a) DK-Sor; (b) RU-Fyo; (c) IT-Cpz; (d) IT-Noe; (e) AT-Neu; (f) US-SRG; (g) CH-Oe2 and (h) US-Ne3. The blue and orange lines are based on B-A and S-S functions, respectively. The title of each panel represents the FLUXNET site ID and vegetation type. Note that modelled lines from S-S and B-A are overlapped in (h). DBF, deciduous broadleaf forest; ENF, evergreen needleleaf forest; EBF, evergreen broadleaf forest; SH, shrub; GRA-C$_3$, C$_3$ grassland; GRA-C$_4$, C$_4$ grassland; CRO-C$_3$, C$_3$ crop; CRO-C$_4$, C$_4$ crop.

function appears to be inadequate for capturing the temperature response of Re during heatwave years, providing underestimated Re in normal temperature ranges and overestimated Re during high-temperature periods. The average temperature across sites for this shift is $20.70 \pm 3.52°C$. The average E_a across sites was underestimated by 0.24 ± 0.12 eV. Interestingly, slightly better performance is found for the B-A function at the US-Ne3 C_4 cropland site (Figure 4h).

3.3 | Biophysical factors influencing E_a and T_{th} in global biomes

Among the explored biophysical variables, T_{th}^{Re}, VPD, MAT, GST and T_{max} exhibit significant influences for all biomes on the activation energy of Re (E_a^{Re}) (Figure 5a). E_a^{Re} and T_{th} of GPP (T_{th}^{GPP}) appear to have the greatest influence on T_{th} of Re (T_{th}^{Re}) across all biomes (Figure 5b). T_{th}^{Re}, T_{max}, MAT, and VPD are found to be significant in affecting the difference in activation energy (ΔE_a^{Re}) across all biomes (Figure 5c). There is no significant correlation between T_{th} and ΔE_a^{Re} (Figure S1). Soil characteristics have relatively low contributions on modelling E_a^{Re} and T_{th}^{Re}.

The ranking of influencing factors for E_a^{Re}, T_{th}^{Re}, and ΔE_a^{Re} varies among biomes (Figure 5). In tropical biome A, PET and AP are the most crucial factors for E_a^{Re}, while SM and AP are the primary factors for T_{th}^{Re}. For ΔE_a^{Re}, T_{th}^{Re} and AP are the key influencing factors. In the polar biome ET, VPD and AP are the primary factors for E_a^{Re}, AP is the main factor for T_{th}^{Re}, and VPD and PET are the most influential factors for ΔE_a^{Re}. Such disparities in factor importance are also observed in other biomes.

3.4 | Discrepancies in the simulated Re by the two functions under future scenarios

The B-A function appears inadequate for capturing the temperature response of Re when temperatures exceed T_{th}, resulting in underestimated Re under normal temperatures and overestimated Re during high-temperature periods. Based on the NoreSM2-MM model simulation, the global number of days with temperature exceeding T_{th} ($T > T_{th}$), where T_{th} is fitted separately for each biome (Figure S6), is projected to increase under all four future scenarios during 2015–2100 (Figure 6a). Specifically, the number of days with $T > T_{th}$ shows a consistent upward trend under the SSP370 and SSP585 scenarios,
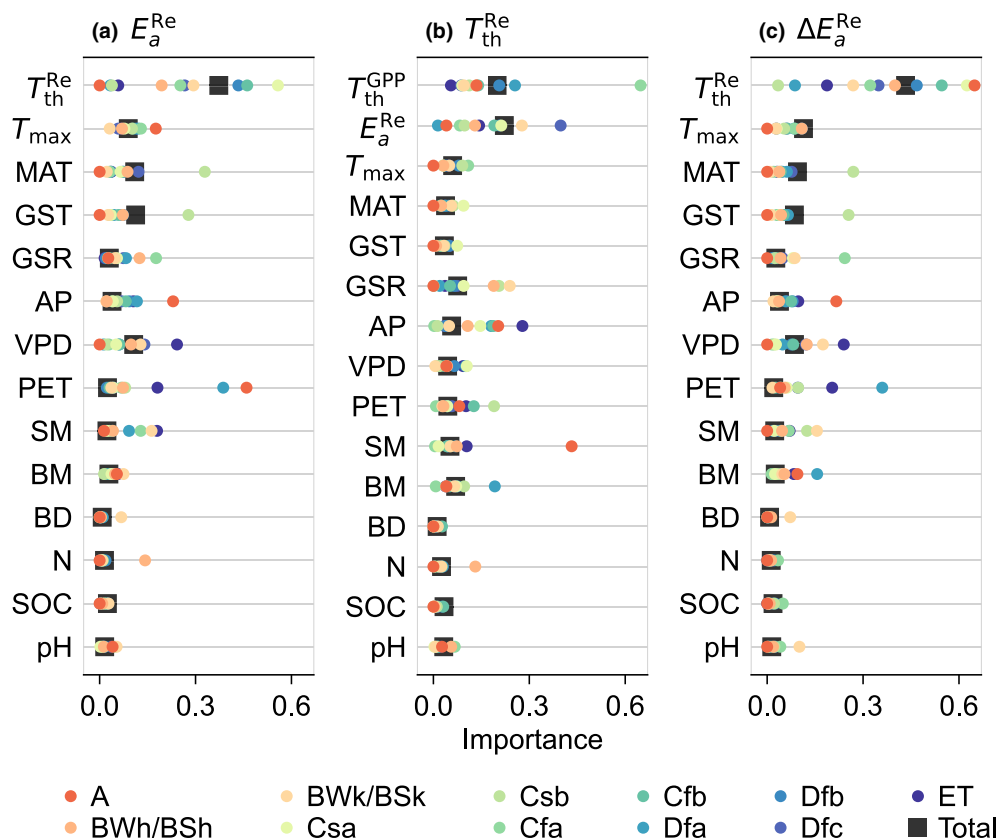

FIGURE 5 Ranked factors influencing the estimation of (a) activation energy (E_a^{Re}) and (b) temperature threshold (T_{th}^{Re}) in the S-S function, and (c) the difference ΔE_a^{Re} between values derived from the S-S and B-A functions, based on random forest analysis. ΔE_a^{Re} represents the difference between the estimated E_a^{Re} from S-S and B-A functions, respectively. T_{th}^{GPP} (°C): Temperature threshold of GPP; T_{max} (°C); MAT (°C); AP (mm); GSR (W m^{-2}); VPD (kPa); PET (mm); SM (%); GST (°C); BD (kg m^{-3}); N (cg kg^{-1}); SOC (g kg^{-1}); pH; BM (Mg C ha^{-1}). Information for model accuracy of random forest is presented in Figures S4 and S5.
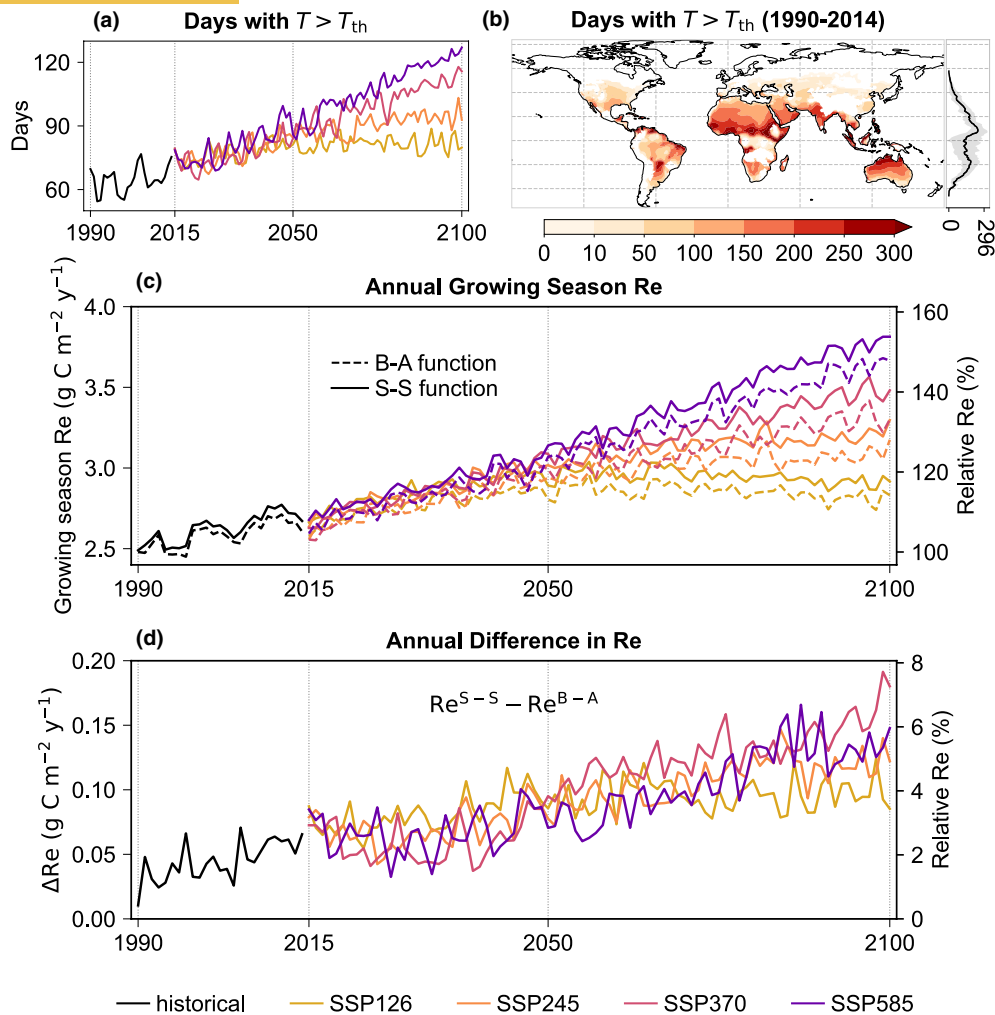
FIGURE 6 Temporal dynamics of Re and air temperature in global biomes, excluding non-vegetated areas, such as built-up lands, snow, ice, barren lands, and water bodies. (a) Annual number of days with temperature exceeding T_{th} in global biomes under four CMIP6 scenarios from 1990 to 2100. (b) Annual number of days with temperatures exceeding T_{th}, based on historical (1990–2014) NoreSM2-MM data, where T_{th} was identified by biome. The insert panel represents the changes in mean $\pm$ std. with latitude. (c) Annual global mean Re during the growing season under the four temperature scenarios from 1990 to 2100. Dashed and solid lines represent the simulated Re based on the B-A and S-S functions, respectively. (d) Annual differences in Re under the four CMIP6 scenarios, calculated as the Re from the S-S function minus that from the B-A function. Re^{B-A} and Re^{S-S} represent the Re simulated using the B-A and S-S functions, respectively. The right axes in (c) and (d) show values normalized to the simulated 1990 Re from the B-A function.

while the increasing rate slows under SSP245 and SSP126 approximately after the mid-21st century (2045–2055). Notably, under the SSP126 scenario, the global average number of days with $T > T_{th}$ stabilizes after the mid-21st century. During the historical period (1990–2014), a pronounced latitudinal gradient is observed, with high values in tropical and subtropical regions (Figure 6b), averaging 65 ± 93 days above T_{th}. Across all four future scenarios, spatial patterns of changes in the number of days with $T > T_{th}$ in the mid- or late-21st (2090–2100) century, relative to those of the historical period remain similar, with the most significant increases occurring in low-latitude regions (Figure S7).

The mean daily Re during the growing-season predicted by the S-S function generally increases faster than those predicted by the B-A function under the four scenarios during 2015–2100 (Figure 6c). This could be attributed to the future increase in days with $T > T_{th}$

(Figure 6a). Under the SSP585 scenario, the predicted mean daily growing-season Re could reach $3.67\,g\,C\,m^{-2}\,y^{-1}$ and $3.81\,g\,C\,m^{-2}\,y^{-1}$ predicted by the B-A and S-S functions, respectively, by 2100 (Figure 6c). They increase by 47.85% and 53.81%, respectively, relative to those in the year 2015. Furthermore, the differences between Re^{B-A} and Re^{S-S} were more clearly demonstrated in Figure 6d. The SSP370 and SSP245 scenarios exhibit a greater average difference, particularly pronounced during the mid-21st century.

4 | DISCUSSION

Departures from exponential behaviour in respiration have been recognized in various modelling research. Heskel et al. (2016) and O'Sullivan et al. (2017) found convergence in leaf respiration across

biomes using a second-order log-polynomial (LP) function, whereas Liang et al. (2018) fitted the temperature response of respiration enzymes using the macromolecular rate theory (MMRT) function. The MMRT function provides a thermodynamic explanation for the temperature dependence of respiration and captures the decline in respiration at high temperatures by introducing the concept of $\Delta C_p^{\ddagger}$, though it is not directly comparable to the E_a of Re in prior research (Yvon-Durocher et al., 2012). Moreover, the MMRT function is mathematically closely related to the LP function, which makes it less flexible in describing the decline in respiration at high temperatures. In contrast, the S-S function, while maintaining the definition of E_a, introduces a more flexible high-temperature inhibition term, represented by E_h, derived from the change in enthalpy of high-temperature inactivation (Schoolfield et al., 1981), and T_h, describing the temperature (K) at which the respiration is half operational and half dormant (Gibert & De Jong, 2001). Through this high-temperature inhibition term, the S-S function can effectively describe all three different types of temperature response of Re: a monotonous increase, an increase followed by a plateau and a unimodal response (Niu et al., 2024). The S-S function also offers the advantage of reduced correlation between parameter estimators (Schoolfield et al., 1981), compared to the MMRT equation (Liang et al., 2018).

The average T_{th} of Re across biomes ranges from 21.21 to 30.95°C, with a mean of 26.58°C, slightly higher than that reported by Chen et al. (2023). However, this range is lower than those reported by O'Sullivan et al. (2017) (50–60°C), Robinson et al. (2017) (60–80°C), and Liang et al. (2018) (64–80°C). Notably, these studies measured T_{th} in artificially heated leaves, laboratory soil and enzyme activity, which may differ from the T_{th} for Re. The T_{th} for Re is a composite concept that may involve various mechanisms, such as the composition of and changes in land cover (Concilio et al., 2005), short supply of respiratory substrates (Chen et al., 2023; Lloyd & Taylor, 1994), inhibition of soil water content (Ma et al., 2005; Wang et al., 2014), thermal adaptation of microbial growth (Maes et al., 2024), thermodynamic properties of enzymes and adenylate control of electron transport (Atkin et al., 2000) acting individually or in combination (Davidson & Janssens, 2006).

Reduced photosynthesis due to high temperatures may constrain Re by limiting the replenishment of nonstructural carbohydrate storage, thereby influencing the temperature response of Re (Allen et al., 2005; Yvon-Durocher et al., 2012). The temperature dependence of photosynthesis is weaker than that of respiration (Jenkinson et al., 1991; Padfield et al., 2016) and is estimated to be approximately 0.32 eV based on exponential function (Allen et al., 2005) and 0.53 eV based on S-S function (Michaletz, 2018). Thus, as proposed by Yvon-Durocher et al. (2012), annual ecosystem respiration, Re(T), can be considered as constrained by photosynthesis, P(T). In this case, Re(T) can be approximated by integrating P(T) with temperature variation over time t: $Re(T) = \theta[P(T)] = \theta \int P(T(t))dt$, where $P(T(t))$ represents a unimodal function, and θ is the fraction of GPP respired by autotrophs and heterotrophs. The temperature dependencies of Re may largely reflect the temperature dependence of its respiratory

components under normal ambient temperature but also indirectly incorporate the temperature dependence of photosynthesis when respiratory substrate availability is limited (Atkin & Tjoelker, 2003; Zhang et al., 2024). This framework assumes that allochthonous carbon inputs are much smaller than autochthonous primary production (Chapin et al., 2011) and that heterotrophic respiration consumes most net primary production (Raich & Potter, 1995). Consequently, the predicted decline in Re(T) with increasing temperature partly reflects a reduction in heterotrophic respiration, as heterotrophic respiration increases more rapidly with temperature than autochthonous net primary production (Allen et al., 2005). This mechanism aligns well with previous studies showing that the thermal sensitivity of photosynthesis constrains respiration at the organismal level (Padfield et al., 2016; Schaum et al., 2018). Therefore, the T_{th}^{GPP} is the key determinant of T_{th}^{Re}, as is shown in Figure 5b.

The constrained effect of respiratory substrate availability has been demonstrated in long-term rates, which are weaker compared to short-term rates and are indistinguishable from that of photosynthesis (Vargas et al., 2010; Yvon-Durocher et al., 2012). For short-term Re, previous studies have documented either increasing (Duffy et al., 2021; von Buttlar et al., 2018) or decreasing (Ciais et al., 2005; Reichstein et al., 2007) trends during heatwaves. However, recent research has indicated that extreme high temperatures enhance the constrained effect strength of GPP on respiration, rather than of respiration on GPP, resulting in a synchronous decline in GPP and Re during heatwaves (Ping et al., 2023). Drake et al. (2019) found no change in the ratio of respiration to photosynthesis following experimental warming treatment. This suggests that such constraints may also exist on a short-term scale.

Actual respiration modelling is unlikely to simply link respiration to photosynthesis (Collalti & Prentice, 2019). Compared with the Farquhar biochemical models of photosynthesis, most approaches to modelling respiration are empirical, as respiration involves a series of biochemical processes occurring continuously across all tissues within ecosystems, each with different mechanisms and metabolic relationships (Chen, 2021; Chen et al., 2023; Reich, 2010; Ryan & Asao, 2019). Soil water content can suppress respiration when it decreases below, or increases beyond, certain threshold points (Xu & Qi, 2001). Both drought and waterlogging could limit enzymatic activity, microbial growth (Schimel et al., 2007), decomposition of soil organic matter (Davidson & Janssens, 2006), plant root function (Burton & Pregitzer, 2003) and gas diffusion (Moyano et al., 2013), thus influencing respiration rate. Soil water content can also affect soil temperature, which in turn impacts the metabolic rates of soil organisms and roots (Suseela & Dukes, 2013). Some microbes produce enzymes that function optimally at higher temperatures, thereby increasing the rate of organic matter breakdown and CO_2 release, influencing ecosystem respiration (German et al., 2012). Warmer temperatures typically decrease microbial carbon use efficiency, leading to more carbon being respired as CO_2 rather than being used for growth (Tucker et al., 2013). Very high temperatures typically result in a decline in the sensitivity of plant respiration to temperature, with a change in the demand for adenosine triphosphate (ATP)

suggested as the primary factor responsible for this short-term response of respiration to temperature (Atkin et al., 2000).

There is currently no scientific consensus in current Earth System Models (ESMs) regarding which temperature response functions to utilize (Ali et al., 2016). The temperature response functions in most ESMs remain unchanged, maintaining a monotonously increasing type, even after the update from CMIP5 to CMIP6 (Varney et al., 2022). Such model deficiencies may compromise the predictive capabilities of these models when confronted with extreme and long-term climate warming (Ryan & Asao, 2019). As rising temperatures push more ecosystems toward their thermal optimum, the B-A function increasingly underestimates Re (Figure 6). However, in the SSP585 scenario, a greater overestimation beyond the divergence threshold due to higher temperatures may explain the difference between the B-A and S-S functions that is smaller than in SSP245 and SSP370 (Figure 6d). Exploring temperature response patterns of Re will be crucial for predicting global Re against the backdrop of ongoing global temperature rise (Bond-Lamberty et al., 2024), as Re serves as the primary pathway for CO_2 entering the atmosphere from the terrestrial biosphere.

It is important to note some limitations of this study. We utilized ambient air temperature and total ecosystem CO_2 exchange, which are directly relevant to global warming estimates tracking global mean surface temperature rather than leaf temperature. However, several crucial factors may impact our conclusions. Temperature often covaries with other variables affecting Re, such as nutrient and water availability, and solar radiation (Reichstein et al., 2013). High-temperature inhibition typically occurs over short periods (Qu et al., 2024), and is therefore potentially underrepresented in limited data. The analysis of temporal dynamics of Re across global biomes does not encompass all biomes. In addition, because of the uneven global distribution of flux towers (Chu et al., 2021), our analysis does not encompass all biomes. Our analysis does not account for Re thermal acclimation (Atkin & Tjoelker, 2003), which may underestimate future trends. Yet this hypothesis about thermal acclimation is still highly uncertain because ecosystem adjustments can lag substantially behind the rate of future warming (Huang et al., 2019). Although treating Re as a whole simplifies the respiration processes, this study still provides a paradigm for the development of respiration models.

This study underscores the critical need of incorporating high-temperature inhibition into Re response functions to more accurately capture the effects of rising temperatures on ecosystem respiration. Our findings demonstrate that the S-S unimodal function, with a temperature threshold for Re inhibition at 26.58°C, outperforms the conventional B-A exponential function in capturing temperature sensitivity. The divergences in projected Re between the two response models emphasize the need for refined modelling approaches to improve predictions of carbon dynamics and inform mitigation strategies in a warming climate.

AUTHOR CONTRIBUTIONS

Zhenhai Liu and Shaoqiang Wang conceived the ideas and designed the methodology; Zhenhai Liu conducted the analysis; Zhenhai Liu,

Jiquan Chen and Bin Chen led the writing of the manuscript; Bin Chen and Shaoqiang Wang provided resources and supervised the work. All authors contributed critically to the drafts and gave final approval for publication.

CONFLICT OF INTEREST STATEMENT
The authors declared no competing interests.

DATA AVAILABILITY STATEMENT
All datasets used in this study are publicly available. The FLUXNET2015 dataset is available at https://fluxnet.org/ (Pastorello et al., 2020). The NoreSM2-MM temperature data are available at https://aims2.llnl.gov/search/cmip6/ (Seland et al., 2020). The Koppen-Geiger climate biomes map is available at https://koeppen-geiger.vu-wien.ac.at/ (Rubel et al., 2017). The scripts supporting the results of this study can be found on Zenodo (https://doi.org/10.5281/zenodo.15459879) and GitHub (https://github.com/lzhzlw/ReTempResponsePaper).

ORCID
Zhenhai Liu https://orcid.org/0000-0003-1209-4641

REFERENCES

Adair, C., Kilsby, D. C., & Whittall, P. T. (1989). Comparison of the Schoolfield (non-linear Arrhenius) model and the square root model for predicting bacterial growth in foods. *Food Microbiology*, *6*(1), 7–18. https://doi.org/10.1016/S0740-0020(89)80033-4

Adams, J. (2017). *Climate_indices, an open source python library providing reference implementations of commonly used climate indices*. GitHub. https://github.com/monocongo/climate_indices

Akaike, H. (1998). Information theory and an extension of the maximum likelihood principle. In E. Parzen, K. Tanabe, & G. Kitagawa (Eds.), *Selected papers of Hirotugu Akaike* (pp. 199–213). Springer. https://doi.org/10.1007/978-1-4612-1694-0_15

Ali, A. A., Xu, C., Rogers, A., Fisher, R. A., Wullschleger, S. D., Massoud, E. C., Vrugt, J. A., Muss, J. D., McDowell, N. G., Fisher, J. B., Reich, P. B., & Wilson, C. J. (2016). A global scale mechanistic model of photosynthetic capacity (LUNA V1.0). *Geoscientific Model Development*, *9*(2), 587–606. https://doi.org/10.5194/gmd-9-587-2016

Allen, A. P., Gillooly, J. F., & Brown, J. H. (2005). Linking the global carbon cycle to individual metabolism. *Functional Ecology*, *19*(2), 202–213. https://doi.org/10.1111/j.1365-2435.2005.00952.x

Arrhenius, S. (1889). Über die Reaktionsgeschwindigkeit bei der Inversion von Rohrzucker durch Säuren. *Zeitschrift für Physikalische Chemie*, *4U*(1), 226–248. https://doi.org/10.1515/zpch-1889-0416

Atkin, O. K., Edwards, E. J., & Loveys, B. R. (2000). Response of root respiration to changes in temperature and its relevance to global warming. *New Phytologist*, *147*(1), 141–154. https://doi.org/10.1046/j.1469-8137.2000.00683.x

Atkin, O. K., & Tjoelker, M. G. (2003). Thermal acclimation and the dynamic response of plant respiration to temperature. *Trends in Plant Science*, *8*(7), 343–351. https://doi.org/10.1016/S1360-1385(03)00136-5

Baldocchi, D., Falge, E., Gu, L., Olson, R., Hollinger, D., Running, S., Anthoni, P., Bernhofer, C., Davis, K., Evans, R., Fuentes, J., Goldstein, A., Katul, G., Law, B., Lee, X., Malhi, Y., Meyers, T., Munger, W., Oechel, W., … Wofsy, S. (2001). FLUXNET: A new tool to study the temporal and spatial variability of ecosystem–scale carbon dioxide, water vapor, and energy flux densities. *Bulletin of the American Meteorological Society*, *82*(11), 2415–2434. https://doi.org/10.1175/1520-0477(2001)082<2415:FANTTS>2.3.CO;2

Bennett, A. C., Arndt, S. K., Bennett, L. T., Knauer, J., Beringer, J., Griebel, A., Hinko-Najera, N., Liddell, M. J., Metzen, D., Pendall, E., Silberstein, R. P., Wardlaw, T. J., Woodgate, W., & Haverd, V. (2021). Thermal optima of gross primary productivity are closely aligned with mean air temperatures across Australian wooded ecosystems. *Global Change Biology*, *27*(19), 4727–4744. https://doi.org/10.1111/gcb.15760

Bennett, A. C., Rodrigues De Sousa, T., Monteagudo-Mendoza, A., Esquivel-Muelbert, A., Morandi, P. S., Coelho De Souza, F., Castro, W., Duque, L. F., Flores Llampazo, G., Manoel Dos Santos, R., Ramos, E., Vilanova Torre, E., Alvarez-Davila, E., Baker, T. R., Costa, F. R. C., Lewis, S. L., Marimon, B. S., Schietti, J., Burban, B., … Phillips, O. L. (2023). Sensitivity of south American tropical forests to an extreme climate anomaly. *Nature Climate Change*, *13*(9), 967–974. https://doi.org/10.1038/s41558-023-01776-4

Bond-Lamberty, B., Ballantyne, A., Berryman, E., Fluet-Chouinard, E., Jian, J., Morris, K. A., Rey, A., & Vargas, R. (2024). Twenty years of progress, challenges, and opportunities in measuring and understanding soil respiration. *Journal of Geophysical Research: Biogeosciences*, *129*(2), e2023JG007637. https://doi.org/10.1029/2023JG007637

Bond-Lamberty, B., & Thomson, A. (2010). Temperature-associated increases in the global soil respiration record. *Nature*, *464*(7288), 579–582. https://doi.org/10.1038/nature08930

Burton, A. J., & Pregitzer, K. S. (2003). Field measurements of root respiration indicate little to no seasonal temperature acclimation for sugar maple and red pine. *Tree Physiology*, *23*(4), 273–280. https://doi.org/10.1093/treephys/23.4.273

Chapin, F. S., Matson, P. A., & Vitousek, P. M. (2011). *Principles of terrestrial ecosystem ecology*. Springer. https://doi.org/10.1007/978-1-4419-9504-9

Chen, J. (2021). *Biophysical models and applications in ecosystem analysis: Ecosystem science and applications*. Michigan State University Press. https://doi.org/10.14321/j.ctv1h1vc27

Chen, W., Wang, S., Wang, J., Xia, J., Luo, Y., Yu, G., & Niu, S. (2023). Evidence for widespread thermal optimality of ecosystem respiration. *Nature Ecology & Evolution*, *7*(9), 1379–1387. https://doi.org/10.1038/s41559-023-02121-w

Chu, H., Luo, X., Ouyang, Z., Chan, W. S., Dengel, S., Biraud, S. C., Torn, M. S., Metzger, S., Kumar, J., Arain, M. A., Arkebauer, T. J., Baldocchi, D., Bernacchi, C., Billesbach, D., Black, T. A., Blanken, P. D., Bohrer, G., Bracho, R., Brown, S., … Zona, D. (2021). Representativeness of Eddy-covariance flux footprints for areas surrounding AmeriFlux sites. *Agricultural and Forest Meteorology*, *301-302*, 108350. https://doi.org/10.1016/j.agrformet.2021.108350

Ciais, P., Reichstein, M., Viovy, N., Granier, A., Ogée, J., Allard, V., Aubinet, M., Buchmann, N., Bernhofer, C., Carrara, A., Chevallier, F., De Noblet, N., Friend, A. D., Friedlingstein, P., Grünwald, T., Heinesch, B., Keronen, P., Knohl, A., Krinner, G., … Valentini, R. (2005). Europe-wide reduction in primary productivity caused by the heat and drought in 2003. *Nature*, *437*(7058), 529–533. https://doi.org/10.1038/nature03972

Collalti, A., & Prentice, I. C. (2019). Is NPP proportional to GPP? Waring's hypothesis 20 years on. *Tree Physiology*, *39*(8), 1473–1483. https://doi.org/10.1093/treephys/tpz034

Concilio, A., Ma, S. Y., Li, Q., Moine, J., Chen, J., North, M., Moorhead, D., & Jensen, R. (2005). Soil respiration response to prescribed burning and thinning in mixed-conifer and hardwood forests. *Canadian Journal of Forest Research*, *35*(7), 1581–1591. https://doi.org/10.1139/x05-091

Davidson, E. A., & Janssens, I. A. (2006). Temperature sensitivity of soil carbon decomposition and feedbacks to climate change. *Nature*, *440*(7081), 165–173. https://doi.org/10.1038/nature04514

Drake, J. E., Furze, M. E., Tjoelker, M. G., Carrillo, Y., Barton, C. V. M., & Pendall, E. (2019). Climate warming and tree carbon use efficiency in a whole-tree $^{13}CO_2$ tracer study. *New Phytologist*, *222*(3), 1313–1324. https://doi.org/10.1111/nph.15721

Duffy, K. A., Schwalm, C. R., Arcus, V. L., Koch, G. W., Liang, L. L., & Schipper, L. A. (2021). How close are we to the temperature tipping point of the terrestrial biosphere? *Science Advances*, *7*(3), eaay1052. https://doi.org/10.1126/sciadv.aay1052

German, D. P., Marcelo, K. R. B., Stone, M. M., & Allison, S. D. (2012). The Michaelis–Menten kinetics of soil extracellular enzymes in response to temperature: a cross-latitudinal study. *Global Change Biology*, *18*(4), 1468–1479. https://doi.org/10.1111/j.1365-2486.2011.02615.x

Gibert, P., & De Jong, G. (2001). Temperature dependence of development rate and adult size in drosophila species: Biophysical parameters. *Journal of Evolutionary Biology*, *14*(2), 267–276. https://doi.org/10.1046/j.1420-9101.2001.00272.x

Gregorutti, B., Michel, B., & Saint-Pierre, P. (2017). Correlation and variable importance in random forests. *Statistics and Computing*, *27*(3), 659–678. https://doi.org/10.1007/s11222-016-9646-1

Heskel, M. A., O'Sullivan, O. S., Reich, P. B., Tjoelker, M. G., Weerasinghe, L. K., Penillard, A., Egerton, J. J. G., Creek, D., Bloomfield, K. J., Xiang, J., Sinca, F., Stangl, Z. R., Martinez-de la Torre, A., Griffin, K. L., Huntingford, C., Hurry, V., Meir, P., Turnbull, M. H., & Atkin, O. K. (2016). Convergence in the temperature response of leaf respiration across biomes and plant functional types. *Proceedings of the National Academy of Sciences of the United States of America*, *113*(14), 3832–3837. https://doi.org/10.1073/pnas.1520282113

Huang, M., Piao, S., Ciais, P., Peñuelas, J., Wang, X., Keenan, T. F., Peng, S., Berry, J. A., Wang, K., Mao, J., Alkama, R., Cescatti, A., Cuntz, M., De Deurwaerder, H., Gao, M., He, Y., Liu, Y., Luo, Y., Myneni, R. B., … Janssens, I. A. (2019). Air temperature optima of vegetation productivity across global biomes. *Nature Ecology & Evolution*, *3*(5), 772–779. https://doi.org/10.1038/s41559-019-0838-x

Isaac, P., Cleverly, J., McHugh, I., van Gorsel, E., Ewenz, C., & Beringer, J. (2017). OzFlux data: Network integration from collection to curation. *Biogeosciences*, *14*(12), 2903–2928. https://doi.org/10.5194/bg-14-2903-2017

Jenkinson, D. S., Adams, D. E., & Wild, A. (1991). Model estimates of CO_2 emissions from soil in response to global warming. *Nature*, *351*(6324), 304–306. https://doi.org/10.1038/351304a0

Johnston, A. S. A., Meade, A., Ardö, J., Arriga, N., Black, A., Blanken, P. D., Bonal, D., Brümmer, C., Cescatti, A., Dušek, J., Graf, A., Gioli, B., Goded, I., Gough, C. M., Ikawa, H., Jassal, R., Kobayashi, H., Magliulo, V., Manca, G., … Venditti, C. (2021). Temperature thresholds of ecosystem respiration at a global scale. *Nature Ecology & Evolution*, *5*(4), 487–494. https://doi.org/10.1038/s41559-021-01398-z

Kattge, J., & Knorr, W. (2007). Temperature acclimation in a biochemical model of photosynthesis: a reanalysis of data from 36 species. *Plant, Cell & Environment*, 30(9), 1176–1190. https://doi.org/10.1111/j.1365-3040.2007.01690.x

Khomik, M., Arain, M. A., Liaw, K.-L., & McCaughey, J. H. (2009). Debut of a flexible model for simulating soil respiration–soil temperature relationship: Gamma model. *Journal of Geophysical Research: Biogeosciences*, 114, G03004. https://doi.org/10.1029/2008JG000851

Lasslop, G., Reichstein, M., Papale, D., Richardson, A. D., Arneth, A., Barr, A., Stoy, P., & Wohlfahrt, G. (2010). Separation of net ecosystem exchange into assimilation and respiration using a light response curve approach: Critical issues and global evaluation. *Global Change Biology*, 16(1), 187–208. https://doi.org/10.1111/j.1365-2486.2009.02041.x

Li, J., Pei, J., Fang, C., Li, B., & Nie, M. (2023). Opposing seasonal temperature dependencies of CO_2 and CH_4 emissions from wetlands. *Global Change Biology*, 29(4), 1133–1143. https://doi.org/10.1111/gcb.16528

Liang, L. L., Arcus, V. L., Heskel, M. A., O'Sullivan, O. S., Weerasinghe, L. K., Creek, D., Egerton, J. J. G., Tjoelker, M. G., Atkin, O. K., & Schipper, L. A. (2018). Macromolecular rate theory (MMRT) provides a thermodynamics rationale to underpin the convergent temperature response in plant leaf respiration. *Global Change Biology*, 24(4), 1538–1547. https://doi.org/10.1111/gcb.13936

Liu, Y. Y., Van Dijk, A. I. J. M., De Jeu, R. A. M., Canadell, J. G., McCabe, M. F., Evans, J. P., & Wang, G. (2015). Recent reversal in loss of global terrestrial biomass. *Nature Climate Change*, 5(5), 470–474. https://doi.org/10.1038/nclimate2581

Lloyd, J., & Taylor, J. A. (1994). On the temperature dependence of soil respiration. *Functional Ecology*, 8(3), 315–323. https://doi.org/10.2307/2389824

Ma, S., Chen, J., Butnor, J. R., North, M., Euskirchen, E. S., & Oakley, B. (2005). Biophysical controls on soil respiration in the dominant patch types of an old-growth, mixed-conifer forest. *Forest Science*, 51(3), 221–232.

Maes, S. L., Dietrich, J., Midolo, G., Schwieger, S., Kummu, M., Vandvik, V., Aerts, R., Althuizen, I. H. J., Biasi, C., Björk, R. G., Böhner, H., Carbognani, M., Chiari, G., Christiansen, C. T., Clemmensen, K. E., Cooper, E. J., Cornelissen, J. H. C., Elberling, B., Faubert, P., … Dorrepaal, E. (2024). Environmental drivers of increased ecosystem respiration in a warming tundra. *Nature*, 629, 105–113. https://doi.org/10.1038/s41586-024-07274-7

Michaletz, S. T. (2018). Evaluating the kinetic basis of plant growth from organs to ecosystems. *New Phytologist*, 219(1), 37–44. https://doi.org/10.1111/nph.15015

Moyano, F. E., Manzoni, S., & Chenu, C. (2013). Responses of soil heterotrophic respiration to moisture availability: An exploration of processes and models. *Soil Biology and Biochemistry*, 59, 72–85. https://doi.org/10.1016/j.soilbio.2013.01.002

Nissan, A., Alcolombri, U., Peleg, N., Galili, N., Jimenez-Martinez, J., Molnar, P., & Holzner, M. (2023). Global warming accelerates soil heterotrophic respiration. *Nature Communications*, 14(1), 3452. https://doi.org/10.1038/s41467-023-38981-w

Niu, S., Chen, W., Liáng, L. L., Sierra, C. A., Xia, J., Wang, S., Heskel, M., Patel, K. F., Bond-Lamberty, B., Wang, J., Yvon-Durocher, G., Kirschbaum, M. U. F., Atkin, O. K., Huang, Y., Yu, G., & Luo, Y. (2024). Temperature responses of ecosystem respiration. *Nature Reviews Earth and Environment*, 5, 559–571. https://doi.org/10.1038/s43017-024-00569-3

Niu, S., Luo, Y., Fei, S., Yuan, W., Schimel, D., Law, B. E., Ammann, C., Altaf Arain, M., Arneth, A., Aubinet, M., Barr, A., Beringer, J., Bernhofer, C., Andrew Black, T., Buchmann, N., Cescatti, A., Chen, J., Davis, K. J., Dellwik, E., … Zhou, X. (2012). Thermal optimality of net ecosystem exchange of carbon dioxide and underlying mechanisms. *New*

Phytologist, 194(3), 775–783. https://doi.org/10.1111/j.1469-8137.2012.04095.x

O'Sullivan, O. S., Heskel, M. A., Reich, P. B., Tjoelker, M. G., Weerasinghe, L. K., Penillard, A., Zhu, L., Egerton, J. J. G., Bloomfield, K. J., Creek, D., Bahar, N. H. A., Griffin, K. L., Hurry, V., Meir, P., Turnbull, M. H., & Atkin, O. K. (2017). Thermal limits of leaf metabolism across biomes. *Global Change Biology*, 23(1), 209–223. https://doi.org/10.1111/gcb.13477

Padfield, D., Castledine, M., & Buckling, A. (2020). Temperature-dependent changes to host–parasite interactions alter the thermal performance of a bacterial host. *The ISME Journal*, 14(2), 389–398. https://doi.org/10.1038/s41396-019-0526-5

Padfield, D., Yvon-Durocher, G., Buckling, A., Jennings, S., & Yvon-Durocher, G. (2016). Rapid evolution of metabolic traits explains thermal adaptation in phytoplankton. *Ecology Letters*, 19(2), 133–142. https://doi.org/10.1111/ele.12545

Papale, D. (2020). Ideas and perspectives: Enhancing the impact of the FLUXNET network of eddy covariance sites. *Biogeosciences*, 17(22), 5587–5598. https://doi.org/10.5194/bg-17-5587-2020

Pastorello, G., Trotta, C., Canfora, E., Chu, H., Christianson, D., Cheah, Y.-W., Poindexter, C., Chen, J., Elbashandy, A., Humphrey, M., Isaac, P., Polidori, D., Reichstein, M., Ribeca, A., van Ingen, C., Vuichard, N., Zhang, L., Amiro, B., Ammann, C., … Papale, D. (2020). The FLUXNET2015 dataset and the ONEFlux processing pipeline for eddy covariance data. *Scientific Data*, 7(1), 225. https://doi.org/10.1038/s41597-020-0534-3

Ping, J., Cui, E., Du, Y., Wei, N., Zhou, J., Wang, J., Niu, S., Luo, Y., & Xia, J. (2023). Enhanced causal effect of ecosystem photosynthesis on respiration during heatwaves. *Science Advances*, 9(43), eadi6395. https://doi.org/10.1126/sciadv.adi6395

Poggio, L., De Sousa, L., Batjes, N., Heuvelink, G., Kempen, B., Ribeiro, E., & Rossiter, D. (2021). SoilGrids 2.0: Producing soil information for the globe with quantified spatial uncertainty. *The Soil*, 7, 217–240. https://doi.org/10.5194/soil-7-217-2021

Qu, L.-P., Chen, J., Xiao, J., De Boeck, H. J., Dong, G., Jiang, S.-C., Hu, Y.-L., Wang, Y.-X., & Shao, C.-L. (2024). The complexity of heatwaves impact on terrestrial ecosystem carbon fluxes: Factors, mechanisms and a multi-stage analytical approach. *Environmental Research*, 240, 117495. https://doi.org/10.1016/j.envres.2023.117495

R Core Team. (2023). *R: A language and environment for statistical computing.* R Foundation for Statistical Computing. https://www.R-project.org/

Raich, J. W., & Potter, C. S. (1995). Global patterns of carbon dioxide emissions from soils. *Global Biogeochemical Cycles*, 9(1), 23–36. https://doi.org/10.1029/94GB02723

Reich, P. B. (2010). The carbon dioxide exchange. *Science*, 329(5993), 774–775. https://doi.org/10.1126/science.1194353

Reichstein, M., Bahn, M., Ciais, P., Frank, D., Mahecha, M. D., Seneviratne, S. I., Zscheischler, J., Beer, C., Buchmann, N., Frank, D. C., Papale, D., Rammig, A., Smith, P., Thonicke, K., van der Velde, M., Vicca, S., Walz, A., & Wattenbach, M. (2013). Climate extremes and the carbon cycle. *Nature*, 500(7462), 287–295. https://doi.org/10.1038/nature12350

Reichstein, M., Ciais, P., Papale, D., Valentini, R., Running, S., Viovy, N., Cramer, W., Granier, A., Ogée, J., Allard, V., Aubinet, M., Bernhofer, C., Buchmann, N., Carrara, A., Grünwald, T., Heimann, M., Heinesch, B., Knohl, A., Kutsch, W., … Zhao, M. (2007). Reduction of ecosystem productivity and respiration during the European summer 2003 climate anomaly: a joint flux tower, remote sensing and modelling analysis. *Global Change Biology*, 13(3), 634–651. https://doi.org/10.1111/j.1365-2486.2006.01224.x

Reichstein, M., Falge, E., Baldocchi, D., Papale, D., Aubinet, M., Berbigier, P., Bernhofer, C., Buchmann, N., Gilmanov, T., Granier, A., Grunwald, T., Havrankova, K., Ilvesniemi, H., Janous, D., Knohl, A., Laurila, T., Lohila, A., Loustau, D., Matteucci, G., … Valentini, R. (2005). On the separation of net ecosystem exchange into assimilation and

ecosystem respiration: Review and improved algorithm. *Global Change Biology*, 11(9), 1424–1439. https://doi.org/10.1111/j.1365-2486.2005.001002.x

Robinson, J. M., O'Neill, T. A., Ryburn, J., Liang, L. L., Arcus, V. L., & Schipper, L. A. (2017). Rapid laboratory measurement of the temperature dependence of soil respiration and application to changes in three diverse soils through the year. *Biogeochemistry*, 133(1), 101–112. https://doi.org/10.1007/s10533-017-0314-0

Rubel, F., Brugger, K., Haslinger, K., & Auer, I. (2017). The climate of the European Alps: Shift of very high resolution Köppen-Geiger climate zones 1800–2100. *Meteorologische Zeitschrift*, 26(2), 115–125. https://doi.org/10.1127/metz/2016/0816

Ryan, M. G., & Asao, S. (2019). Clues for our missing respiration model. *New Phytologist*, 222(3), 1167–1170. https://doi.org/10.1111/nph.15805

Schaum, C.-E., Barton, S., Bestion, E., Buckling, A., Garcia-Carreras, B., Lopez, P., Lowe, C., Pawar, S., Smirnoff, N., Trimmer, M., & Yvon-Durocher, G. (2017). Adaptation of phytoplankton to a decade of experimental warming linked to increased photosynthesis. *Nature Ecology & Evolution*, 1(4), 0094. https://doi.org/10.1038/s41559-017-0094

Schaum, C.-E., Buckling, A., Smirnoff, N., Studholme, D. J., & Yvon-Durocher, G. (2018). Environmental fluctuations accelerate molecular evolution of thermal tolerance in a marine diatom. *Nature Communications*, 9(1), 1719. https://doi.org/10.1038/s41467-018-03906-5

Schimel, D. S., House, J. I., Hibbard, K. A., Bousquet, P., Ciais, P., Peylin, P., Braswell, B. H., Apps, M. J., Baker, D., Bondeau, A., Canadell, J., Churkina, G., Cramer, W., Denning, A. S., Field, C. B., Friedlingstein, P., Goodale, C., Heimann, M., Houghton, R. A., … Wirth, C. (2001). Recent patterns and mechanisms of carbon exchange by terrestrial ecosystems. *Nature*, 414(6860), 169–172. https://doi.org/10.1038/35102500

Schimel, J., Balser, T. C., & Wallenstein, M. (2007). Microbial stress-response physiology and its implications for ecosystem function. *Ecology*, 88(6), 1386–1394. https://doi.org/10.1890/06-0219

Schoolfield, R. M., Sharpe, P. J. H., & Magnuson, C. E. (1981). Non-linear regression of biological temperature-dependent rate models based on absolute reaction-rate theory. *Journal of Theoretical Biology*, 88(4), 719–731. https://doi.org/10.1016/0022-5193(81)90246-0

Seland, Ø., Bentsen, M., Olivié, D., Toniazzo, T., Gjermundsen, A., Graff, L. S., Debernard, J. B., Gupta, A. K., He, Y.-C., Kirkevåg, A., Schwinger, J., Tjiputra, J., Aas, K. S., Bethke, I., Fan, Y., Griesfeller, J., Grini, A., Guo, C., Ilicak, M., … Schulz, M. (2020). Overview of the Norwegian earth system model (NorESM2) and key climate response of CMIP6 DECK, historical, and scenario simulations. *Geoscientific Model Development*, 13(12), 6165–6200. https://doi.org/10.5194/gmd-13-6165-2020

Stinziano, J. R., Way, D. A., & Bauerle, W. L. (2018). Improving models of photosynthetic thermal acclimation: Which parameters are most important and how many should be modified? *Global Change Biology*, 24(4), 1580–1598. https://doi.org/10.1111/gcb.13924

Suseela, V., & Dukes, J. S. (2013). The responses of soil and rhizosphere respiration to simulated climatic changes vary by season. *Ecology*, 94(2), 403–413. https://doi.org/10.1890/12-0150.1

Tagesson, T., Kelly, J., Schurgers, G., Tian, F., Ardö, J., Horion, S., Ahlström, A., Olin, S., & Fensholt, R. (2024). Increasing global ecosystem respiration between 1982 and 2015 from earth observation-based modelling. *Global Ecology and Biogeography*, 33(1), 116–130. https://doi.org/10.1111/geb.13775

Tang, R., He, B., Chen, H. W., Chen, D., Chen, Y., Fu, Y. H., Yuan, W., Li, B., Li, Z., Guo, L., Hao, X., Sun, L., Liu, H., Sun, C., & Yang, Y. (2022). Increasing terrestrial ecosystem carbon release in response to autumn cooling and warming. *Nature Climate Change*, 12(4), 380–385. https://doi.org/10.1038/s41558-022-01304-w

Todd-Brown, K. E. O., Randerson, J. T., Post, W. M., Hoffman, F. M., Tarnocai, C., Schuur, E. A. G., & Allison, S. D. (2013). Causes of variation in soil carbon simulations from CMIP5 earth system models and comparison with observations. *Biogeosciences*, 10(3), 1717–1736. https://doi.org/10.5194/bg-10-1717-2013

Tucker, C. L., Bell, J., Pendall, E., & Ogle, K. (2013). Does declining carbon-use efficiency explain thermal acclimation of soil respiration with warming? *Global Change Biology*, 19(1), 252–263. https://doi.org/10.1111/gcb.12036

Vargas, R., Baldocchi, D. D., Allen, M. F., Bahn, M., Black, T. A., Collins, S. L., Yuste, J. C., Hirano, T., Jassal, R. S., Pumpanen, J., & Tang, J. (2010). Looking deeper into the soil: Biophysical controls and seasonal lags of soil CO_2 production and efflux. *Ecological Applications*, 20(6), 1569–1582. https://doi.org/10.1890/09-0693.1

Varney, R. M., Chadburn, S. E., Burke, E. J., & Cox, P. M. (2022). Evaluation of soil carbon simulation in CMIP6 earth system models. *Biogeosciences*, 19(19), 4671–4704. https://doi.org/10.5194/bg-19-4671-2022

Vickers, D., Thomas, C. K., Martin, J. G., & Law, B. (2009). Self-correlation between assimilation and respiration resulting from flux partitioning of eddy-covariance CO_2 fluxes. *Agricultural and Forest Meteorology*, 149(9), 1552–1555. https://doi.org/10.1016/j.agrformet.2009.03.009

von Buttlar, J., Zscheischler, J., Rammig, A., Sippel, S., Reichstein, M., Knohl, A., Jung, M., Menzer, O., Arain, M. A., Buchmann, N., Cescatti, A., Gianelle, D., Kiely, G., Law, B. E., Magliulo, V., Margolis, H., McCaughey, H., Merbold, L., Migliavacca, M., … Mahecha, M. D. (2018). Impacts of droughts and extreme-temperature events on gross primary production and ecosystem respiration: a systematic assessment across ecosystems and climate zones. *Biogeosciences*, 15(5), 1293–1318. https://doi.org/10.5194/bg-15-1293-2018

Wang, X., Liu, L., Piao, S., Janssens, I. A., Tang, J., Liu, W., Chi, Y., Wang, J., & Xu, S. (2014). Soil respiration under climate warming: Differential response of heterotrophic and autotrophic respiration. *Global Change Biology*, 20(10), 3229–3237. https://doi.org/10.1111/gcb.12620

Xu, H., Xiao, J., & Zhang, Z. (2020). Heatwave effects on gross primary production of northern mid-latitude ecosystems. *Environmental Research Letters*, 15(7), 074027. https://doi.org/10.1088/1748-9326/ab8760

Xu, M., & Qi, Y. (2001). Soil-surface CO_2 efflux and its spatial and temporal variations in a young ponderosa pine plantation in northern California. *Global Change Biology*, 7(6), 667–677. https://doi.org/10.1046/j.1354-1013.2001.00435.x

Yu, P., Zhou, T., Luo, H., Liu, X., Shi, P., Zhang, Y., Zhang, J., Zhou, P., & Xu, Y. (2022). Global pattern of ecosystem respiration tendencies and its implications on terrestrial carbon sink potential. *Earth's Future*, 10(8), e2022EF002703. https://doi.org/10.1029/2022EF002703

Yvon-Durocher, G., Caffrey, J. M., Cescatti, A., Dossena, M., del Giorgio, P., Gasol, J. M., Montoya, J. M., Pumpanen, J., Staehr, P. A., Trimmer, M., Woodward, G., & Allen, A. P. (2012). Reconciling the temperature dependence of respiration across timescales and ecosystem types. *Nature*, 487(7408), 472–476. https://doi.org/10.1038/nature11205

Zhang, S., Wang, M., Xiao, L., Guo, X., Zheng, J., Zhu, B., & Luo, Z. (2024). Reconciling carbon quality with availability predicts temperature sensitivity of global soil carbon mineralization. *Proceedings of the National Academy of Sciences*, 121(11), e2313842121. https://doi.org/10.1073/pnas.2313842121

Zou, H., Chen, J., Shao, C., Dong, G., Duan, M., Zhu, Q., & Li, X. (2022). Model selection for ecosystem respiration needs to be site specific: Lessons from grasslands on the Mongolian plateau. *Land*, 11(1), 87. https://doi.org/10.3390/land11010087

Functional Ecology

SUPPORTING INFORMATION

Additional supporting information can be found online in the Supporting Information section at the end of this article.

Figure S1. Distribution of E_a ($n = 159$) by range and threshold temperature.

Figure S2. Spatial changes of estimated parameters based on B-A and S-S functions. The insert in each panel represents the latitudinal changes.

Figure S3. Distribution of T_{th} ($n = 159$) for all FLUXNET2015 sites.

Figure S4. Comparisons between the observed and estimated T_{th}^{Re} and E_a^{Re} of the testing dataset in the random forest model.

Figure S5. Comparisons between the observed and modeled ΔE_a^{Re} of the testing dataset in the random forest model.

Figure S6. Modeled average ecosystem respiration (Re) based on B-A and S-S functions across global biomes.

Figure S7. Spatial patterns of changes in cumulative days with $T > T_{th}$ for mid- or late-21st century compared to those of the historical period (1990–2014) under the four CMIP6 scenarios.

Table S1. The search space of each parameter for each fit used in our fitting work.

Table S2. Estimated model coefficients for sites with better fitting from the B-A function.